Inorg. Chem. **2005**, *44*, 6004–6011

Crystal Structures and Magnetic Properties of Complexes of $M^{II}Cl_2$ (M = Cu, Ni, and Co) Coordinated with 4-(*N*-*tert*-butyloxyamino)-2-(methoxymethylenyl)pyridine: 2D Magnetic Anisotropy of the Aminoxyl-Co^{II} Complex in the Crystalline State

Zhicheng Zhu, Satoru Karasawa, and Noboru Koga*

Graduate School of Pharmaceutical Sciences, Kyushu University, Maidashi 3-1-1, Higashi-Ku, Fukuoka, Japan, 812−8582

Received November 5, 2004

Three metal complexes, [$M^{II}Cl_2$(**4NOPy-OMe**)$_2$] (M = Cu (**1**), Ni (**2**), and Co (**3**)), were prepared by mixing the corresponding metal chloride and 4-(*N*-*tert*-butyloxyamino)-2-(methoxymethylenyl)pyridine, **4NOPy-OMe**, in 1:2 ratio. Complex **1** has two structures (complexes **A** and **B**) with similar coordination geometries, compressed octahedrons. In the crystal structure, complexes **A** and **B** locate alternately in short distances ($C_{radical}\cdots C_{\beta}$ = 3.17 and 3.23 Å) to form a 1-D chain structure. Complexes **2** and **3** are isomorphous and have a slightly distorted octahedral structure. In the crystal structure, both complexes have intermolecular short contacts ($C_{radical}\cdots C_{\alpha}$ = 3.46 and 3.52 Å for **2** and **3**, respectively) to form the 2-D structures. The temperature dependence of the $\chi_{mol}T$ values for the three complexes indicated that the magnetic interactions between the radicals and the metal ions within the complexes were ferromagnetic. By fitting a modified Fisher 1-D model to the data of the $\chi_{mol}T$ vs T plot for **1**, we estimated the intra- and intermolecular (intrachain) exchange coupling constants to be J_1/k_B = 60.2 and J_2/k_B = –7.02 K, respectively. On the other hand, complexes **2** and **3** showed steep increases of the $\chi_{mol}T$ value below ca. 3 K, indicating that the long-range magnetic ordering is operating. The $1/\chi_{mol}$ vs T plot for **2** was analyzed by a Curie–Weiss model to give θ = 6.25 K and C = 2.02 cm^3 K mol^{-1} with g_{Ni} = 2.25. Complex **3** was investigated in more detail using an orientated sample. Magnetic behavior strongly depends on the direction of the applied field, in which the *c** axis perpendicular to the *ab* plane is an easy axis for magnetization. Direct current (dc) and alternating current (ac) magnetic susceptibility measurements revealed that complex **3** had a magnetic phase transition of T_c = 2.14 K and exhibited a glasslike magnetic behavior below T_c.

Introduction

Low-dimensional assemblies of anisotropic metal ions having one- and two-dimensional (1-D and 2-D) structures have been noted in the field of molecule-based magnets.[1] They show magnetic behavior similar to that of the classical magnet having three-dimensional (3-D) spin orderings. The typical examples of 1-D complexes in low-dimensional assemblies are single-chain magnets (SCMs)[2] exhibiting slow magnetic relaxation. The 2-D assemblies have been also investigated intensively, and the magnetic behaviors strongly affected by magnetic anisotropy resulting from the structure and the metal ion itself have been reported.[3]

For the construction of single-molecule magnets (SMMs),[4] which have a 0-D structure, we proposed the use of a hetero-spin system[5] consisting of the 2p spins of organic radicals and the 3d spins of metal ions. The 1:4 heterospin complex

* To whom correspondence should be addressed. E-mail: koga@fc.phar.kyushu-u.ac.jp. Fax: +81-92-642-6590.

(1) Benelli, C.; Gatteschi, D. *Chem. Rev.* **2002**, *102*, 2369. (b) Kahn, O. *Acc. Chem. Res.* **2000**, *33*, 647. (c) Ohba, M.; Okawa, H. *Coord. Chem. Rev.* **2000**, *198*, 313. (d) Miller, J. S.; Epstein, A. J.; Reiff, W. M. *Chem. Rev.* **1988**, *88*, 201.

(2) Wang, S.; Zuo, J.; Gao, S.; Song, Y.; Zhou, H.; Zhang, Y.; You, X. *J. Am. Chem. Soc.* **2004**, *126*, 8900. (b) Miyasaka, H.; Clérac, R.; Mizushima, K.; Sugiura, K.; Yamashita, M.; Wernsdorfer, W.; Coulon, C. *Inorg. Chem.* **2003**, *42*, 8203. (c) Clérac, R.; Miyasaka, H.; Yamashita, M.; Coulon, C. *J. Am. Chem. Soc.* **2002**, *124*, 12837. (d) Caneschi, A.; Gatteschi, D.; Lalioti, N.; Sangregorio, C.; Sessoli, R.; Venturi, G.; Vindigni, A.; Rettori, A.; Pini, M. G.; Novak, M. A. *Angew. Chem., Int. Ed.* **2001**, *40*, 1760.

(3) Miyasaka, H.; Ieda, H.; Masamoto, N.; Sugiura, K.; Yamashita, M. *Inorg. Chem.* **2003**, *42*, 3509. (b) Larionova, J.; Kahn, O.; Gohlen, S.; Ouahab, L.; Clérac, R. *J. Am. Chem. Soc.* **1999**, *121*, 3349. (c) Larionova, J.; Kahn, O.; Golhen, S.; Ouahab, L.; Clérac, R. *Inorg. Chem.* **1999**, *38*, 3621.

10.1021/ic048441x CCC: $30.25
Published on Web 07/22/2005

Table 1. Crystallographic Data and Experimental Parameters for **1**, **2**, and **3**

	1	**2**	**3**
empirical formula	$CuC_{22}H_{34}N_4O_4Cl_2$	$NiC_{22}H_{34}N_4O_4Cl_2$	$CoC_{22}H_{34}N_4O_4Cl_2$
fw	552.99	548.129	548.369
a (Å)	23.662(5)	20.05(2)	20.132(3)
b (Å)	8.931(2)	11.14(1)	11.218(3)
c (Å)	24.759(3)	14.25(1)	16.201(3)
α (deg)	90	90	90
β (deg)	103.23(1)	127.10(3)	135.128(8)
γ (deg)	90	90	90
V (Å^3)	5093(1)	2539(3)	2581.5(8)
Z	8	4	4
space group	*C*2/*c* (No. 15)	*C*2/*c* (No. 15)	*C*2/*c* (No. 15)
T (K)	123 ± 1	123 ± 1	123 ±1
λ (Å)	0.71069	0.71069	0.71069
D_{calcd} (g cm^{-3})	1.442	1.434	1.411
μ (Mo Kα) (cm^{-1})	1.102	1.009	0.906
unique reflns	6170	3036	3103
no. observed	4783	936	2340
no. variables	335	209	167
GOF	1.111	1.590	1.405
R^a	0.050	0.032	0.034
$R_w{}^b$	0.082	0.052	0.070

[a] $R = \sum||F_0| - |F_c||/\sum|F_0|$. [b] $R_w = [\sum w (F_0^2 - F_c^2)^2/\sum w(F_0^2)^2]^{1/2}$

of $Co^{(II)}(NCO)_2$ coordinated with pyridine ligands carrying an aminoxyl radical, **4NOPy**, showed an SMM magnetic behavior with a relatively large activation barrier for the reorientation of the spins, $U_{eff}/k_B = 50$ K in frozen solution.[6] An analogous cobalt complex with pyridine carrying a carbene, **1CPy**, also showed a similar SMM behavior with $U_{eff}/k_B = 89$ K in frozen solution.[7] In these works, the SMM behaviors were observed only in frozen solution conditions. No observations in the crystalline states are the result of the intermolecular magnetic interaction. For example, [Co-$(NCO)_2$·(**4NOPy**)$_4$], which exhibits SMM behavior in frozen solution, had the intermolecular short contacts to form a 3-D structure and showed antiferromagnet-like behavior in the crystalline state.[6b] Although the intermolecular magnetic interaction in the crystalline state is undesirable for a SMM, the interaction can be regarded as the formation of a new spin network. This time, we noted the short contacts of the spin centers with the neighboring molecules, which were frequently observed in the crystal structure of heterospin complexes,[5b,5c,6] and considered taking advantage of the intermolecular interaction for the construction of a low-dimensional assembly. Since the unique magnetic behaviors of low-dimensional complexes strongly depend on the magnetic anisotropy of the metal ion itself,[2,3] the selection of the metal ion is important. On the basis of our studies of SMMs,[6,7] a high-spin cobalt(II) ion was selected and a new bidentate pyridine ligand carrying an aminoxyl radical, 4-(*N*-*tert*-butyloxyamino)-2-(methoxymethylenyl)pyridine, **4NOPy-OMe**, was designed. The use of a bidentate pyridine ligand, **4NOPy-OMe** results in a decrease in the number of organic spin centers in the complex, and the stability of the octahedral structure of the complex in solution at room temperature will be improved. A discrete cobalt(II) complex, [$Co^{(II)}Cl_2$·(**4NOPy-OMe**)$_2$], in the crystalline state was expected to form a low-dimensional network and show unique magnetic behavior affected by the magnetic anisotropy of the cobalt-(II) ion.

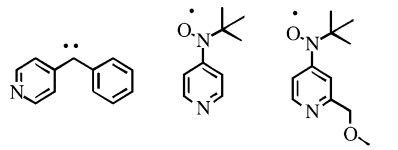

1CPy **4NOPy** **4NOPy-OMe**

In addition, to understand the effect of the anisotropy of the metal ion, we prepared complexes of copper and nickel ions with weak magnetic anisotropy via the reaction of **4NOPy-OMe** with the corresponding $M^{II}Cl_2$. The crystal structures and magnetic properties of the 1:2 complexes, [M^{II}-Cl_2·(**4NOPy-OMe**)$_2$] (M = Cu (**1**), Ni (**2**), and Co (**3**)), were investigated by X-ray crystal structure analysis and SQUID magnetosusceptometry, respectively.

Experimental Section

General. ^{1}H NMR (270 MHz) spectra were recorded on a JEOL 270 Fourier Transform Spectrometer using $CDCl_3$ as the solvent and referenced to TMS. Infrared spectra were measured on a JASCO FT/IR 420 spectrometer with KBr pellets. UV−vis spectra were obtained on a JASCO V570 spectrometer. EPR spectra were performed on a Bruker ESP300 X-band (9.4 GHz) spectrometer. FAB mass spectra were recorded on a JEOL JMS−SX102 spectrometer. Melting points were obtained with a MEL-TEMP heating block and are uncorrected. Elemental analysis was performed in the analytical center of Kyushu University.

X-ray Crystal and Molecular Structure Analyses. Crystallographic data and experimental details for complexes **1**, **2**, and **3** are summarized in Table 1. Suitable single crystals were glued onto a glass fiber using epoxy resin. All X-ray data were collected on a Rigaku Raxis-Rapid diffractometer with graphite monochromated Mo Kα radiation ($\lambda = 0.71069$ Å). Reflections were collected at

(4) Gatteschi, D.; Sessoli, R. *Angew. Chem., Int. Ed.* **2003**, *42*, 268. (b) Sessoli, R.; Gatteschi, D.; Caneschi, A.; Novak, M. A. *Nature* **1993**, *365*, 141.
(5) Koga, N.; Karasawa, S. *Bull. Chem. Soc. Jpn.* **2005**, in press. (b) Ishimaru, Y.; Kitano, M.; Kumada, M.; Koga, N.; Iwamura, H. *Inorg. Chem.* **1998**, *37*, 2273. (c) Kumada, H.; Sakane, A.; Koga, N.; Iwamura, H. *J. Chem. Soc., Dalton Trans*. **2000**, 911.
(6) Kanegawa, S.; Karasawa, S.; Nakano, M.; Koga, N. *Chem. Commun*. **2004**, 1750. (b) Kanegawa, S.; Karasawa, S.; Nakano, M.; Koga, N. To be published.
(7) Karasawa, S.; Zhou, G.; Morikawa, H.; Koga, N. *J. Am. Chem. Soc*. **2003**, *125*, 13676.

123 ± 1 K. The structures were solved by direct methods (SIR92) and expanded using Fourier techniques (DIRDIF94). The refinements were converged using the full-matrix least-squares method from the Crystal Structure software package[8] to give the *C*2/*c* (No. 15) space group for the complexes. All non-hydrogen atoms were refined anisotropically. Hydrogen atoms were found by standard methods or from the differential electron map and refined isotropically.

Measurements of Magnetic Properties. Magnetic susceptibility data (ac and dc) were obtained on Quantum Design MPMS2 and MPMS5S SQUID magnetosusceptometers, respectively, and corrected for the magnetization of the sample holder and capsule and the diamagnetic contributions to the samples, which were estimated from Pascal's constants.[9] A pulverized sample was prepared by grinding crystals of the complex to powder and restrained by cotton in a sample capsule to avoid partial reorientation of the crystal during magnetic measurement. For the magnetic measurement of a direction-arranged sample of **3**, a single crystal ($0.8 \times 0.5 \times 0.3$ mm^3) was selected and used. The axis orientation of the crystal was determined by X-ray analysis, and then the crystal was arranged on a sample holder. Dc magnetic susceptibilities were measured by a sequence of ZFCM (zero field-cooled magnetization), FCM (field-cooled magnetization), and RM (remnant magnetization) at a dc field of 4.6 Oe; ac measurements were carried out with a 1 Oe oscillating field with a zero dc field at the frequencies of 1, 10, 100, 500, and 1000 Hz.

Preparations of Ligand and Complexes. Unless otherwise stated, the preparative reactions were carried out under a high-purity dry nitrogen atmosphere. Ether and THF (tetrahydrofuran) were distilled from sodium benzophenone ketyl. 4-Bromo-pyridylcarbinol[10] and 2-methyl-2-nitrosopropane[11] were prepared and purified by modified procedures reported in the literature.

4-Bromo-2-(methoxymethylenyl)pyridine. NaH (60% in mineral oil, 2.0 g, 50.0 mmol) was added to a solution of 4-bromo-2-pyridylcarbinol (3.47 g, 18.5 mmol) in dry THF (50 mL). The mixture was stirred vigorously at 50 °C for 15 min. After the mixture was cooled to room temperature, dry methyl iodide (2.4 mL, 38.6 mmol) was added, and the mixture was stirred for an additional 2 h. After the usual workup, the brown crude product was chromatographed on silica gel with $CHCl_3$ as the eluent to give 4-bromo-2-(methoxymethylenyl)pyridine (3.0 g, 80.1% yield) as colorless oil. ^{1}H NMR (270 MHz, $CDCl_3$): δ 8.36 (1H, s), 7.62 (1H, s), 7.37 (1H, d), 4.57 (2H, s), 3.49 (3H, s). FAB MS (in *m*-NBA matrix): 202.1, 204.1 (M + 1). Anal. Calcd for C_7H_8NOBr: C, 41.61; H, 3.99; N, 6.93. Found: C, 41.67; H, 4.02; N, 6.89.

4-(*N*-*tert*-butyl-*N*-hydroxyamine)-2-methoxymethylenylpyridine. A 1.6 M solution of *n*-butyllithium in *n*-hexane (6.1 mL) was added through a syringe over a period of 10 min to a solution of 4-bromo-2-(methoxymethylenyl)pyridine (1.53 g, 7.57 mmol) in dry ether (40 mL) at −78 °C. After the mixture was stirred for 30 min, a solution of 2-methyl-2-nitrosopropane (1.36 g, 15.8 mmol) in dry ether (20 mL) was added dropwise. The reaction mixture was stirred for 1h, and the dry ice bath was removed. After the usual workup, a brown oil was obtained. The crude oil was chromatographed on silica gel with AcOEt/*n*-hexane as the eluent to give hydroxylamine as an off-white waxy solid (1.00 g, 62.5% yield). mp: 65−67 °C. ^{1}H NMR (270 MHz, $CDCl_3$): δ 8.22 (1H, d), 7.29 (1H, s), 7.10 (1H, d), 4.47 (2H, s), 3.38 (3H, s), 1.20 (9H, s). FAB MS (in *m*-NBA matrix): 211.2 (M + 1). Anal. Calcd for $C_{11}H_{18}N_2O_2$: C, 62.83; H, 8.63; N, 13.32. Found: C, 62.87; H, 8.79; N, 13.24.

4-(*N*-*tert*-butyloxyamino)-2-(methoxymethylenyl)pyridine (4NOPy-OMe). Freshly prepared Ag_2O (1.2 g, 52.0 mmol) was added to a solution of 4-(*N*-*tert*-butyl-*N*-hydroxyamine)-2-methoxymethylenylpyridine (640 mg, 3.0 mmol) in ether (100 mL). The mixture was stirred at room temperature until all the hydroxyamine disappeared. After filtration through a short alumina column, a red ethereal solution of a radical was obtained. The radical was found to be stable in solution under a nitrogen atmosphere, while it was unstable in the oily solid state. Therefore, the solution of the radical was used for the spectra and magnetic measurements and for the complexation with MCl_2 immediately after preparation without isolation and purification. UV−vis (ether): λ = 293, 368, and 525 (shoulder) nm. EPR (ether): a_N = 10.5 G; g = 2.0067.

[$CuCl_2$·(4NOPy-OMe)$_2$] (1). An ethereal solution of **4NOPy-OMe** (20 mL, ca. 1 mmol) was added to a solution of $CuCl_2 \cdot 2H_2O$ (85 mg, 0.5 mmol) in acetonitrile (5 mL). The mixture was condensed to 4 mL under reduced pressure and filtered. The brown filtrate was kept in an atmosphere of ether vapor in a refrigerator. Copper complex **1** was obtained as a dark brown block crystal (129 mg, 46.0% yield). mp (decomp): 141−143 °C. Anal. Calcd for $CuC_{22}H_{34}N_4O_4Cl_2$: C, 47.78; H, 6.20; N, 10.13. Found: C, 47.87; H, 6.16; N, 10.25.

[$NiCl_2$·(4NOPy-OMe)$_2$] (2). The complex was prepared in a manner similar to that used for **1** using 119 mg of $NiCl_2 \cdot 6H_2O$ instead of $CuCl_2 \cdot 2H_2O$. Single crystals (199 mg, 72.6%) were obtained by slow diffusion of ether vapor into the solution of the complex. mp (decomp): 145−148 °C. Anal. Calcd $NiC_{22}H_{24}N_4O_4Cl_2$: C, 48.21; H, 6.25; N, 10.22. Found: C, 48.17; H, 6.27; N, 10.45.

[$CoCl_2$·(4NOPy-OMe)$_2$] (3). The complex was prepared in a manner similar to that used for **1** using 119 mg $CoCl_2 \cdot 6H_2O$ instead of $CuCl_2 \cdot 2H_2O$. Single crystals (216 mg, 78.8% yield) were obtained by slow diffusion of ether vapor into the solution of the complex. mp (decomp): 141−143 °C. Anal.Calcd for $CoC_{22}H_{34}N_4O_4Cl_2$: C, 48.19; H, 6.25; N, 10.22. Found: C, 48.02; H, 6.24; N, 10.21.

Results and Discussion

Synthesis and General Properties. The bidentate ligand carrying an aminoxyl radical, **4NOPy-OMe**, was obtained as an orange-red ethereal solution after oxidation of the corresponding hydroxylamine derivative with Ag_2O. The aminoxyl radical center in **4NOPy-OMe** was stable at −30 °C in ether for several days but not in condensed solution. Therefore, the ethereal radical solution was used for the complexation with the metal ion immediately after the preparation without isolation and purification. Complexations were achieved by mixing a radical solution and a metal chloride hydrate solution in a molar ratio of 2:1. Slow diffusion of ether vapor into the solutions of the complexes in acetonitrile produced single crystals in high yields. Complexes, **1**, **2**, and **3**, obtained as dark brown plateau-shaped bricks, orange-red prisms, and dark red block crystals, respectively, were perfectly stable in the atmosphere.

(8) For SIR92, see: Altomare, A.; Cascarano, G.; Giacovazzo, C.; Guagliardi, A.; Burla, M.; Polidori, G.; Camalli, M. *J. Appl. Crystallogr.* **1994**, *27*, 435. (b) Beurskens, P. T.; Admiraal, G.; Beurskens, G.; Bosman, W. P.; de Gelder, R.; Israel, R.; Smits, J. M. M. *DIRDIF99*; Crystallography Laboratory, University of Nijmegen: The Netherlands, 1994. (c) *CrystalStructure*, version 3.5.1; Rigaku and Rigaku/MSC: The Woodlands, 2000−2003.

(9) Kahn, O. *Molecular Magnetism*; VCH Publishers: Weinheim, Germany, 1993.

(10) Ashimori, A.; Ono, T.; Uchida, T.; Ohtaki, Y.; Fukaya, C.; Watanabe, M.; Yokoyama, K. *Chem. Pharm. Bull.* **1990**, *38*, 2446. (b) Tamura, M.; Urano, Y.; Kikuchi, K.; Higuchi, T.; Hirobe, M.; Nagano, T. *Chem. Pharm. Bull.* **2000**, *48*, 1514. (c) Suzuki, I. *Yakugaku Zasshi* **1948**, *68*, 126; *Chem. Abstr.* **1953**, *47*, 8074.

(11) Stowell, J. C. *J. Org. Chem.* **1971**, *36*, 3055.

Table 2. Selected Bond Lengths (Å), Bond Angles (deg), and Dihedral Angles (deg)

Bond Lengths (Å)

1				2		3	
Cu1−Cl1	2.3004(9)	Cu2−Cl2	2.300(1)	Ni−Cl	2.368(3)	Co−Cl	2.3738(7)
Cu2−Cl3	2.336(1)						
Cu1−N1	2.005(2)	Cu2−N3	1.984(2)	Ni−N1	2.07(1)	Co−N1	2.124(3)
Cu1−O2	2.477(3)	Cu2−O4	2.549(3)	Ni−O2	2.143(6)	Co−O2	2.188(2)
N2−O1	1.292(5)	N4−O3	1.280(4)	N2−O1	1.28(1)	N2−O1	1.271(3)
N2−C3	1.417(4)	N4−C15	1.414(4)	N2−C3	1.43(2)	N2−C3	1.425(5)

Bond Angles (deg)

1				2		3	
O1−N2−C3	116.3(3)	O3−N4−C14	116.0(3)	O1−N2−C3	115.0(1)	O1−N2−C3	115.9(3)
O2−Cu1−O2′	173.87	O4−Cu2−O4′	180	O2−Ni−O2′	78.51(4)	O2−Co−O2′	75.84(6)
Cl1−Cu1−Cl1′	180	Cl3−Cu2−Cl3′	180	Cl1−Ni−Cl2	103.27(6)	Cl1−Co−Cl1′	107.88(2)
Cl1−Cu1−O2	89.80(7)	Cl3−Cu2−O4	86.79(6)	Cl1−Ni−O2	89.95(5)	Cl−Co−O2	89.73(2)
N1−Cu1−N1′	178.35	N3−Cu2−N3′	180	N1−Ni−N3	172.54(4)	N1−Co−N1′	172.92(6)
				Cl1−Ni−N1	88.98(2)	Cl1−Co−N1	89.50(6)
				N1−Ni−O2	75.65(5)	N1−Co−O2	73.58(9)

Dihedral Angles (deg)[a]

1				2		3	
O1−N2−C3-py	13.68,	O3−N4−C15-py	17.63	O1−N2−C3-py	40.07	O1−N2−C3-py	38.74

[a] Dihedral angle between radical plane and pyridine ring (defined as the plane of C1−C3−C5 or C12−C14−C16).

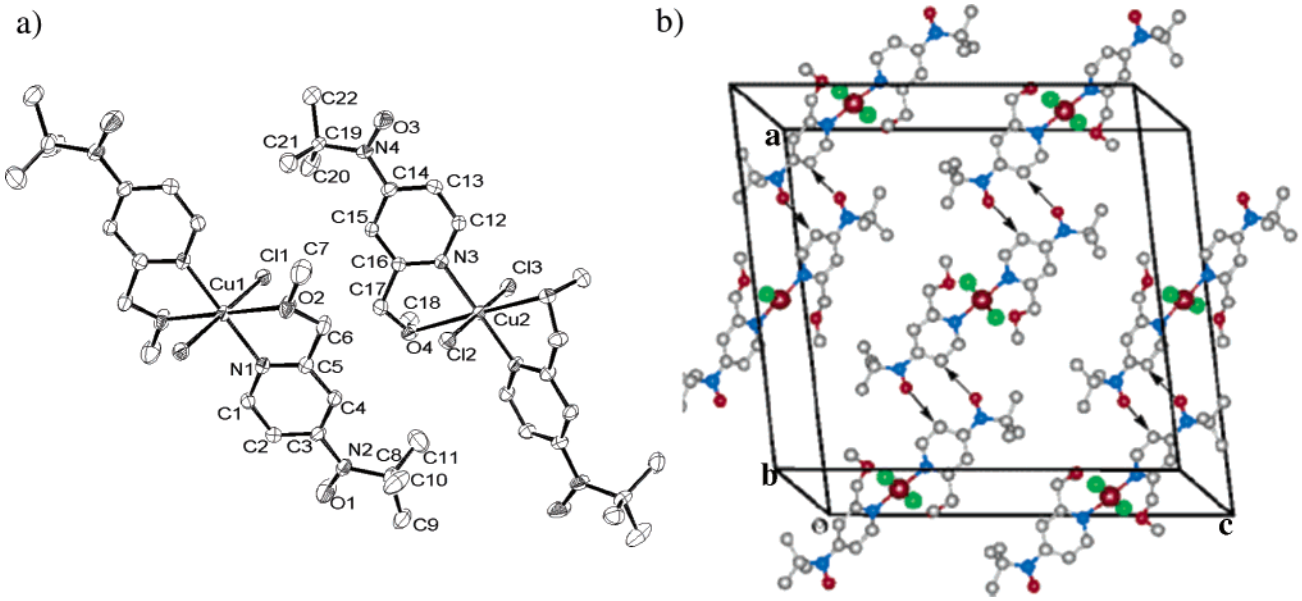

Figure 1. (a) ORTEP drawing of the molecular structure of **1** (units **A** and **B**) with the atom numbering scheme showing 30% probability ellipsoids and (b) a ball-and-stick model for the 1-D chain structure of **1**. The arrow indicates the intermolecular short contact.

X-ray Crystal and Molecular Structures. The molecular and crystal structures for complexes **1**, **2**, and **3** were analyzed by X-ray structure analysis. Selected bond lengths and bond angles are listed in Table 2.

[$CuCl_2$·(4NOPy-OMe)$_2$] (1). A perspective view of **1** is depicted in Figure 1a together with the selected atom numbering scheme. Complex **1** consists of two copper complexes, units **A** and **B**, with slightly different geometries. The symmetries for units **A** and **B** have an inverse center at the Cu1 atom and a 2-fold axis through Cl2−Cu2−Cl3, respectively. In both units, two pyridine nitrogen atoms, two chloride anions, and two methoxy oxygen atoms are coordinated to the copper(II) ion in a strict trans configuration. The copper ions reside in the center of the compressed octahedron, in which the bond lengths are Cu1−N1 = 2.005 Å, Cu1−Cl1 = Cu1−Cl1′ = 2.300 Å, and Cu1−O2 = 2.477 Å for unit **A** and Cu2−N3 = 1.984 Å, Cu2−Cl2 = 2.300 Å, Cu2−Cl3 = 2.336 Å, and Cu2−O4 = 2.549 Å for unit **B**. The Cu−O bond lengths observed in both units are rather long, indicating that the oxygen of the methoxy ligands bound weakly. The two pyridine rings are almost coplanar in unit **A** and are twisted around each other by 29.70° in unit **B**. The dihedral angles between the pyridine ring and the radical plane, which are defined as O1−N2−C3 for unit **A** and O3−N4−Cl4 for unit **B**, are 13.68° and 17.63°, respectively.

As shown in Figure 1b, the intermolecular short contacts between the oxygen atoms of aminoxyl and β carbon of the pyridine ring were found in the distance of 3.17 and 3.23 Å,

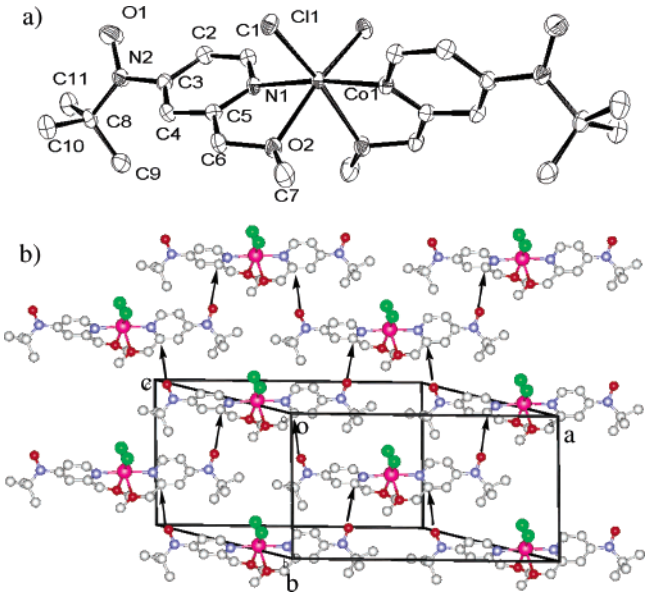

Figure 2. (a) ORTEP drawing of the molecular structure of **3** with the atom numbering scheme showing 30% probability ellipsoids and (b) a ball-and-stick model for the 2-D layer structure of **3** along the *ab* plane. The arrows indicate the intermolecular short contacts.

which connect unit **A** with unit **B** alternately to form a 1-D magnetic chain. There is no short distance within 4 Å between the chains to suggest a magnetic interaction.

[$NiCl_2$·(4NOPy-OMe)$_2$] (2) and [$CoCl_2$·(4NOPy-OMe)$_2$] (3). The molecular and crystal structures of complexes **2** and **3** are isomorphous with similar bond lengths and angles as listed in Table 2. The molecular structure and the crystal packing of **3** are shown in Figure 2a and b, respectively.

The molecular structures for both complex **2** and **3** have a 2-fold axis passing through the six-coordinated center metal ions. The metal ion resides in the center of the octahedral coordination structure in which the bond lengths of M−Cl, M−N, and M−O are 2.37, 2.07, and 2.14 Å for **2** (M = Ni) and 2.37, 2.12, and 2.19 Å for **3** (M = Co), respectively. Pyridine nitrogen atoms are coordinated to the metal ions in a trans configuration, while the chloride and methoxy oxygen atoms are in a cis configuration. In both **2** and **3**, the dihedral angle between two pyridine planes, which are nearly perpendicular to each other, and the pyridine ring and the aminoxyl plane is 40.70° for **2** and 38.74° for **3**. The latter dihedral angles are relatively large, suggesting that the magnetic coupling between the aminoxyl center and the metal ion through the pyridine ring might be weaker than that for copper complex **1**.

As shown in Figure 2b, each complex molecule is connected with four neighboring molecules by short contact to form a 2-D layer along the *ab* plane. The intermolecular distances between the oxygen atoms of aminoxyl and the α carbon (C5) of the neighboring pyridine ring are 3.46 Å for **2** and 3.52 Å for **3**. In the layered structure, two kinds of the plane exist: the molecules in one plane align in one direction and the others align in the opposite direction. They are layered alternately along the *c* axis,

Magnetic Properties. [$CuCl_2$·(4NOPy-OMe)$_2$] (1). The magnetic susceptibility for the microcrystalline sample of **1**

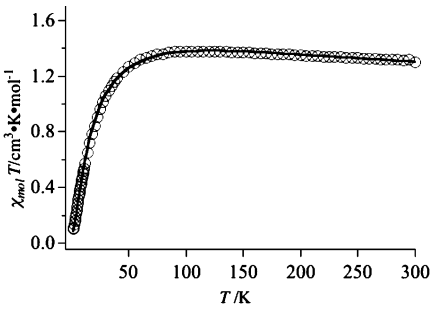

Figure 3. Plot of $\chi_{mol}T$ vs T for the pulverized sample of **1**. The solid curve is a theoretical one.

Scheme 1

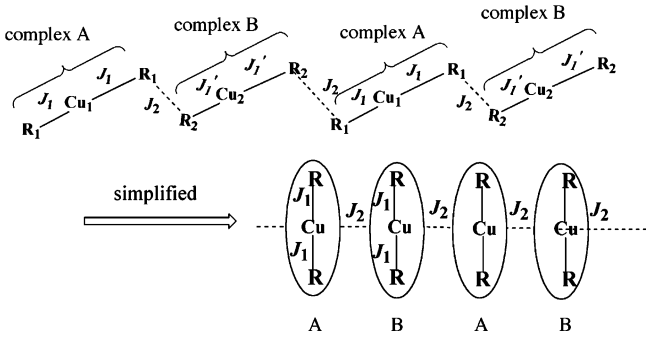

was measured in the temperature range of 2−300 K at the constant field of 5 kOe. The temperature dependence of $\chi_{mol}T$ is shown in Figure 3.

The $\chi_{mol}T$ value at 300 K was about 1.30 cm^3 K mol^{-1}, which was slightly larger than the theoretical value ($\chi_{mol}T$ = 1.13 cm^3 K mol^{-1}) calculated for three isolated spins with S = 1/2 in terms of the spin-only equation. As the temperature decreased, the $\chi_{mol}T$ value increased gradually, reaching a maximum of 1.38 cm^3 K mol^{-1} at 100 K, and then when the temperature was below 50 K, the $\chi_{mol}T$ value decreased steeply to 0.1 cm^3 K mol^{-1}at 1.9 K. The increase of the $\chi_{mol}T$ values observed in 300−100 K range indicates that the magnetic interactions between the aminoxyls and the copper ion through the pyridine rings are ferromagnetic. On the other hand, the decrease of the $\chi_{mol}T$ values below 100 K indicates that antiferromagnetic interactions take place intermolecularly (within the chain).

To elucidate magnetic interactions in **1** quantitatively, the spin model of the 1-D chain repeating the radical−Cu−radical units was considered (Scheme 1), in which the difference in magnetic interaction between complex **A** and **B** was assumed to be negligible and the parameters, J_1 and J_2, were the exchange coupling parameters for intra- and intermolecular (within the chain) interactions, respectively.

The modified Fisher 1-D model reported in the literature[12] was applied for this spin system. The Hamiltonian can be written as $H_{chain} = -J\sum S_T S_{T+1}$, where S_T represents temperature-dependent spin of the radical−Cu−radical species. The temperature dependence of the magnetic susceptibility is given by eq 1 where all symbols have the usual meaning.

(12) Li, L.; Liao, D.; Jiang, Z.; Yan, S. *Inorg. Chem.* **2002**, *41*, 421. (b) Li, L.; Liao, L.; Liu, S.; Jiang, Z.; Yan, S. *Inorg. Chem. Commun.* **2003**, *6*, 225.

$$x_{\text{chain}} = \frac{N\mu_B{}^2 g^2}{3kT} S_T(S_T+1)\frac{1+u}{1-u} \quad (1)$$

$$u = \coth[J_2 S_T(S_T+1)/kT] - [kT/J_2 S_T(S_T+1)]$$

$$S_T(S_T+1) = 3kx_T T/Ng^2\mu_B{}^2$$

$$x_T = \frac{N\mu_B{}^2 g^2}{3kT}\frac{60\exp(3J_1/T)+6\exp(2J_1/T)+6}{4[4\exp(3J_1/T)+2\exp(2J_1/T)+2]}$$

The fitting of eq 1 to the experimental data was refined by means of a least-squares method. The best fitting parameters are 60.2 ± 1.5 and −7.02 ± 0.08 K for J_1 and J_2, respectively. The theoretical curve is shown by a solid line in Figure 3. The signs of J_1 and J_2 indicate that the magnetic interaction between the aminoxyls and the copper ion is ferromagnetic and that the magnetic interaction between the molecules is antiferromagnetic. The former J_1 value for intramolecular coupling between two aminoxyls and the copper ion is close to that (60.4 K) for [Cu(hfac)$_2$·(**4NOPy**)$_2$].[5b] Note that the intermolecular interaction within the chain (J_2 value is negative) is antiferromagnetic and that the nearest points between the molecules are the radical center and the β carbon of the pyridine ring of the neighboring molecule.

[NiCl$_2$·(4NOPy-OMe)$_2$] (2). The molar magnetic susceptibility for the pulverized crystalline sample was measured in temperature ranges of 300−10 and 10−1.9 K at constant fields of 5 and 0.5 kOe, respectively. The temperature dependence of $\chi_{\text{mol}}T$ is shown in Figure 4.

The $\chi_{\text{mol}}T$ value at 300 K was about 2.08 cm^3 K mol^{-1}, which was larger than the spin-only value ($\chi_{\text{mol}}T$ = 1.75 cm^3 K mol^{-1}) calculated for three isolated spins (S = 1/2 for aminoxyls and S = 2/2 for a high-spin nickel(II) ion). As the temperature decreased, the $\chi_{\text{mol}}T$ value gradually increased to 2.34 cm^3 K mol^{-1} at 50 K, and then the $\chi_{\text{mol}}T$ value steeply increased at temperatures below 10 K. The value of 9.53 cm^3 K mol^{-1} at 1.9 K exceeds that (3.00 cm^3 K mol^{-1}) for S = 4/2. The observed thermal profile of the $\chi_{\text{mol}}T$ values above 50 K and below 10 K indicates that intra- and intermolecular ferromagnetic interactions, respectively, take place. The steep increase of $\chi_{\text{mol}}T$ values below 3 K suggests the onset of a long-range magnetic ordering. The data between 300 and 50 K have been fitted through the Curie−Weiss law, $\chi_{\text{mol}}{}^{-1} = (T-\theta)/C$ (inset of Figure 4). The fit gives C = 2.02 cm^3 K mol^{-1}, θ = 6.25 K, and g_{Ni} = 2.25 (g_{radical} = 2.00 is fixed). The field dependence of magnetization, M, was measured at 1.90 K up to 50 kOe (Figure S1). When the outer field increased, the M value began to reach the saturation magnetization, M_s, but not completely, even at 50 kOe. The value of 3.76 Nμ_B at 50 kOe is close to that of M_s, which is 4.25 Nμ_B, for g_{radical} = 2.00 and g_{Ni} = 2.25 with S = 4/2.

To characterize the long-range magnetic ordering of complex **2**, we performed dc magnetic measurements, using a sequence of zero field-cooled magnetization (ZFCM) and field-cooled magnetization (FCM) measurements, and ac magnetic measurement in the temperature range of 5−1.9 K. In the ZFCM and FCM measurements, no bifurcation of the M values was observed above 1.9 K. In the temperature dependence of in-phase and out-of phase components, χ'_{mol} and χ''_{mol}, respectively, the χ'_{mol} signal gradually increased and the χ''_{mol} signal appeared below ca. 3 K (Figure S2). The small nonzero value of χ''_{mol} suggests that the phase transition for complex **2** might occur below 1.9 K, an inaccessible temperature for our apparatus.

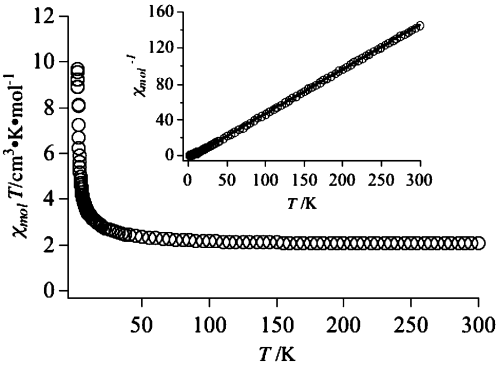

Figure 4. Plot of $\chi_{\text{mol}}T$ vs T for the pulverized crystalline sample of **2**. The inset shows the $\chi_{\text{mol}}{}^{-1}$ vs T plot. The solid line was a theoretical one.

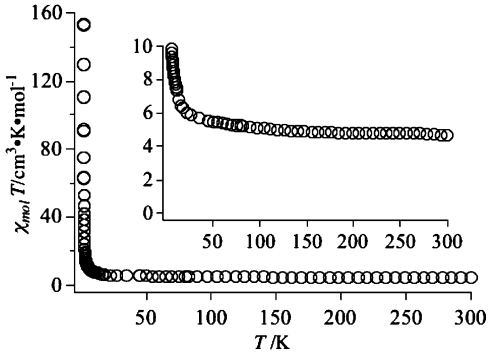

Figure 5. Plot of $\chi_{\text{mol}}T$ vs T of the pulverized crystalline sample for **3**. The inset shows the expansion of $\chi_{\text{mol}}T$ value.

[CoCl$_2$·(4NOPy-OMe)$_2$] (3). In the dc and ac magnetic susceptibility experiments for cobalt complex **3**, pulverized crystalline and single-crystal samples were used.

Pulverized Crystalline Sample. The dc molar magnetic susceptibilities of the pulverized crystalline sample were measured in the temperature ranges of 300−10 and 10−1.9 K at constant fields of 5 and 0.05 kOe, respectively. The temperature dependence of $\chi_{\text{mol}}T$ is shown in Figure 5.

The $\chi_{\text{mol}}T$ value at 300 K is 4.70 cm^3 K mol^{-1}, which is much larger than the spin-only value (2.63 cm^3 K mol^{-1}) for the three isolated spins (S = 1/2 for aminoxyls and S = 3/2 for Co(II) ion). This large difference may be the result of the spin−orbit coupling[9] of Co(II) or the exchange-coupled Co-aminoxyl system. When the temperature decreased, the $\chi_{\text{mol}}T$ value increased gradually up to 50 K (5.50 cm^3 K mol^{-1}), and then the $\chi_{\text{mol}}T$ value increased steeply at temperatures below 5 K. This thermal profile[13] of the $\chi_{\text{mol}}T$ value is similar to that for nickel complex **2**. The steep increase of the $\chi_{mol}T$ value below 5 K and the value of 153 cm^3 K mol^{-1} at 1.9 K indicates a long-range magnetic ordering of the magnetic spin.

(13) The Curie−Weiss equation fitted the data of $1/\chi_{\text{mol}}$ in the temperature range of 300−50 K to give C = 4.59 cm^3 K mol^{-1} and θ = 9.42 K with g_{Co} = 2.86 (g_{radical} = 2.00 was fixed).

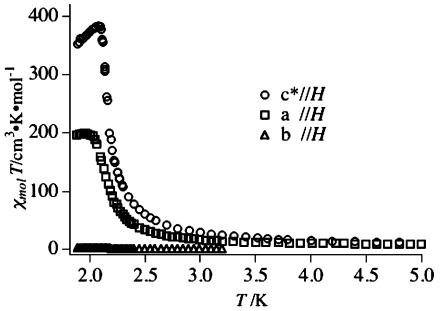

Figure 6. Plot of $\chi_{mol}T$ vs T of the direction-arranged crystalline sample of **3**. The field was applied to $c^*\|H$ (○, H = 4.6 Oe), $a\|H$ (□, H = 100 Oe), and $b\|H$ (△, H = 500 Oe).

Single-Crystal Sample. For the dc and ac magnetic measurements for an oriented sample, a single crystal with the approximate dimension of 0.8 × 0.5 × 0.3 mm (0.22 mg) was selected. The crystal, for which the axis of orientation was determined by X-ray analysis, was mounted on a sample holder. The temperature dependence of $\chi_{mol}T$ of the single-crystal sample was measured at constant fields of 4.6, 100, and 500 Oe applied along the *a*, *b*, and *c** axes, respectively, in the temperature range of 5.0−1.9 K. As observed in the $\chi_{mol}T$ vs T plot (Figure 6), the thermal profile of the $\chi_{mol}T$ value strongly depends on the direction from which the field is applied. When the external field is applied parallel to the *a* and *c** axes, $a\|H$ and $c^*\|H$, respectively, the $\chi_{mol}T$ values increase steeply below 2.2 K, and the $\chi_{mol}T$ value at 1.9 K for $c^*\|H$ was larger than that for $a\|H$. In the field applied along the *b* axis, $b\|H$, on the other hand, the $\chi_{mol}T$ values showed the smallest maximum at 2.1 K. Thus, the direction perpendicular to the *ab* plane, $c^*\|H$, is the easy axis of magnetization. It is interesting that the *a* and *b* axes are the directions of N1···Co···N1 (intramolecular magnetic interaction between Co and the aminoxyl center) and O1···C5′ (intermolecular short contact), respectively.

To fully characterize the long-range magnetic ordering, we performed dc magnetization measurements, using a sequence of zero field-cooled magnetization (ZFC), field-cooled magnetization (FCM), and remnant magnetization (RM), and ac magnetic susceptibility measurements of in-phase and out-of-phase components, χ'_{mol} and χ''_{mol}, respectively, in the temperature range of 5.0−1.9 K. The results below 3 K in both the dc and ac magnetic measurements with the field applied along the easy axis, $c^*\|H$, are shown in Figure 7a and b, respectively.

The M values in the FCM measurements at a constant field of 4.6 Oe increased rapidly at 3.00−2.10 K, reached the value of 822 cm^3 Oe mol^{-1} at 2.1 K, and then slightly increased below that temperature. The derivative curve, dM/dT, of the FCM measurement gave an extremum at the temperature of 2.14 K corresponding to the critical temperature, T_c. In the RM measurement, the M values (60.5 cm^3 Oe mol^{-1} at 1.9 K) were observed and disappeared at temperatures above 2.1 K. A small discrepancy in the M values between the ZFCM and FCM measurements was observed below T_c = 2.14 K. In the ac magnetic susceptibility measurements, both the χ'_{mol} and χ''_{mol} signals, with frequency dependence, were observed as shown in Figure 7b. The thermal profile of χ'_{mol} was similar to that for the FCM measurement with a rapid

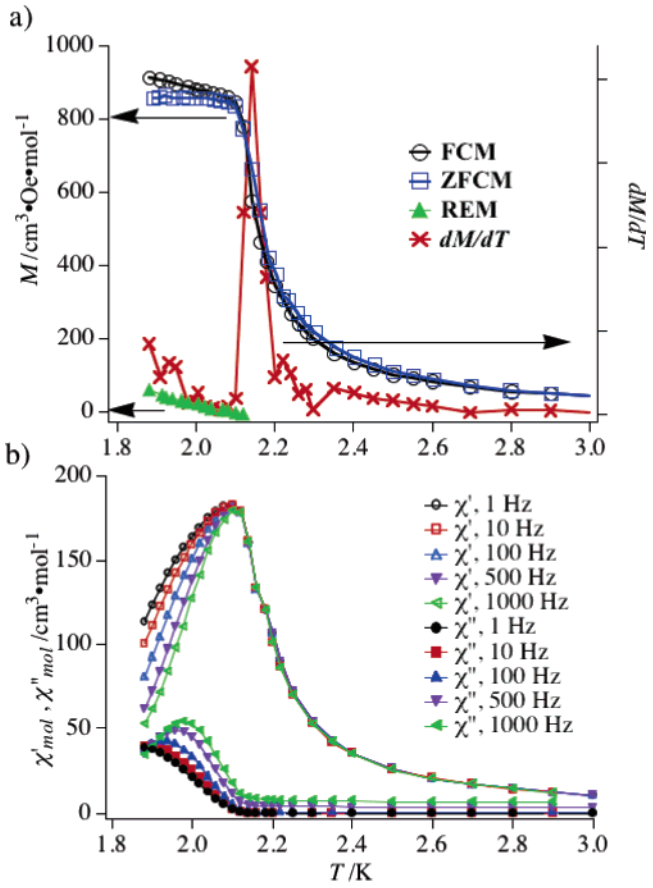

Figure 7. (a) M vs T plot for the ZFCM, FCM, and RM measurements together with the dM/dT curve and (b) χ'_{mol} and χ''_{mol} vs T plots at 1000, 500, 100, 10, and 1 Hz for the single-crystal sample of **3**. The field was applied to $c^*\|H$. Solid lines are guides for the eye.

increase in the temperature range of 3.0−2.1 K. Below 2.1 K, the χ'_{mol} values decreased with frequency dependence. At the same temperature, the χ''_{mol} signals appeared and showed the maximum at each frequency. The peak-top temperatures of χ''_{mol} at each frequency followed the Arrhenius law, $\tau = \tau_0 \exp(\Delta/k_B)$ to give an activation barrier, Δ/k_B, of 154 K and a τ_0 of 1.67 × 10^{-37} s, indicating that complex **3** has a glassy behavior below T_c. The frequency dependence of χ''_{mol} might be explained by the dynamics of the magnetic domain in the ordered phase. Similar magnetic behaviors in 2-D layered[14] and 1-D chain[15] complexes were reported in the literature.

To confirm the ferromagnetic nature of the transition, we measured the field dependence of magnetization at 1.9 K up to 50 kOe. The plots of M vs H for the sample with the field applied to three axes are shown in Figure 8.[16] The magnetization curves strongly depended on the direction of the applied field. A rapid saturation of the magnetization,

(14) Coronado, E.; Gomez-Garcia, C. J.; Nuez, A.; Romero, F. M.; Rusanov, E.; Stoeckli-Evans, H. *Inorg. Chem.* **2002**, *41*, 4615. (b) Bellouard, F.; Clemente-Leon, M.; Coronado, E.; Galan-Mascaros, J. R.; Gomez-Garcia, C. J.; Romero, F.; Dunbar, K. R. *Eur. J. Inorg. Chem.* **2002**, *43*, 1603.

(15) Li, D.; Zheng, L.; Zhang, Y.; Huang, J.; Gao, S.; Tang, W. *Inorg. Chem.* **2003**, *42*, 6123.

(16) Although a weak hystresis (H_c = ~5 Oe) was observed in the M vs H plot for a pulverized sample, it was not observed for an oriented sample. The hysteresis loop might be affected by glassy magnetic behavior observed below T_c.

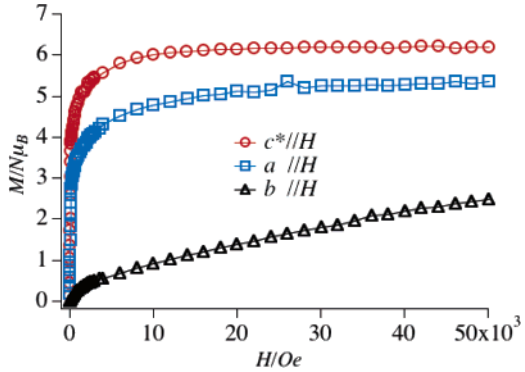

Figure 8. $M/N\mu_B$ vs H plot at 1.9 K for the oriented single-crystal sample. The field was applied to $c^*||H$, $a||H$, and $b||H$. Solid lines are guides for eyes.

M_s, with a value of 6.18 $N\mu_B$ was observed for $c^*||H$, corresponding to the g_{eff} value of 4.12 with $S = 3/2$. On the other hand, M values for $a||H$ and $b||H$ gradually increased to 5.34 and 2.48 $N\mu_B$, respectively, at 50 kOe.

Comparisons of the Magnetic Properties in 1, 2, and 3. In all three complexes, **1**, **2**, and **3**, the intramolecular magnetic interactions between the metal ion and the aminoxyl radical are ferromagnetic. The exchange coupling parameter, J/k_B, was estimated to be 60 K for **1**. The J/k_B values for **2** and **3** might be smaller than that for **1**, which was suggested by the large dihedral angles between the aminoxyl plane and the pyridine ring. On the other hand, the intermolecular interactions are antiferromagnetic for **1** and ferromagnetic for **2** and **3**. The difference of intermolecular magnetic interaction in the three complexes is elucidated by the spin-polarization mechanism.[17] According to the spin-polarization mechanism, in **1**, **2**, and **3**, the same sign (or up spin) as those for the aminoxyl center and the metal ion will be induced at the β carbon of the pyridine ring, while the opposite sign (or down spin) is at the α carbon. Therefore, intermolecular (through-space) magnetic couplings through the β and α carbons of pyridine ($O_{radical}\cdots C_\beta$ and $O_{radical}\cdots C_\alpha$) are expected to become antiferromagnetic and ferromagnetic, respectively. In the crystal packings revealed by X-ray analysis, the nearest atoms to the aminoxyl radical centers are the β carbons of the neighboring pyridine rings for **1** and α carbons for **2** and **3**: **1**, $O_{radical}\cdots C_\beta = 3.17$ and 3.23 Å; **2**, $O_{radical}\cdots C_\alpha = 3.46$ Å; and **3**, $O_{radical}\cdots C_\alpha = 3.52$ Å. The observed magnetic behaviors in the three complexes are consistent with the prediction obtained by the spin-polarization mechanism. Similar proximities between the aminoxyl center and the β carbon of the neighboring pyridine ring ($O\cdots C_\beta$) were observed in the crystal structures of $[Co(NCO)_2(\mathbf{4NOPy})_4]$[6b] and $[M(hfac)_2(\mathbf{4NOPy})_2]$ (M = Cu,[5b] Ni,[18] and Co[18]). They showed the intermolecular antiferromagnetic interactions between the metal ion and the aminoxyl radicals. On the other hand, the proximity of $O\cdots C_\alpha$ was also observed in the crystal of $[Cu(hfac)_2(\mathbf{4NOBpy})_2]$ (Bpy = 2,2′-bipyridine), which showed ferromagnetic interaction.[5c]

Complexes **2** and **3** are isomorphous and show similar magnetic behaviors except for a difference in the magnetic phase transition temperature: T_c is less than 1.9 K for **2** and is 2.14 K for **3**. Since the total magnetic behavior in a low-dimensional complex is strongly affected by both structural and metal-ion anisotropy,[2,3,14,15] the observed difference in T_c in **2** and **3**, which have similar crystal structures, might be the result of the metal anisotropy. The Co(II) ion with a $^4T_1$ local ground state at low temperature has large magnetic anisotropy compared with the Ni(II) ion of $^3A_2$.[9]

Conclusion

The discrete heterospin complexes, $[MCl_2(\mathbf{4NOPy\text{-}OMe})_2]$ (M = Cu (**1**), Ni (**2**), and Co (**3**)), showed magnetic behavior depending on the crystal structure and the metal ion. Complex **1** had intramolecular ferromagnetic interactions and intermolecular (intrachain) antiferromagnetic interactions to form a 1-D magnetic chain. Complexes **2** and **3** are isomorphous. They had the intra- and intermolecular ferromagnetic interactions and showed long-range magnetic orderings below 3 K. In complex **3**, especially, a magnetic phase transition took place at 2.14 K (T_c) and a glasslike magnetic behavior was exhibited below T_c. Furthermore, complex **3** was found to have strong 2-D magnetic anisotropy in which an easy axis is the direction perpendicular to the *ab* plane, the *c** direction. These results clearly indicate that the organic spins, aminoxyls, in the heterospin system effectively operate intra- and intermolecularly to form a low-dimensional spin network. As observed in the magnetic behavior of **3**, the heterospin system containing the cobalt(II) ion will be useful for the study of magnetic anisotropy in low-dimensional assemblies.

Intramolecular interactions will be required to improve the magnetic property of the present heterospin system. For this purpose, a ligand bridging two metal binding sites through organic spins was designed. The preparation of the ligand and its metal complexes are in progress.

Acknowledgment. This work was supported by a Grant-in-Aid for Scientific Research (A)(2)(No.14204071) and a Grant-in-Aid for Scientific Research on Priority Areas "Application of Molecular Spin" (No. 15087205) from the Ministry of Education, Science, Sports and Technology (MEXT), Japan. A part of this work was supported by "Nanotechnology Support Project" of the Ministry of Education, Culture, Sports, Science and Technology, Japan.

Supporting Information Available: X-ray crystallographic file in CIF format for **1**, **2**, and **3**, M vs H plot at 1.9 K, and χ' and χ'' vs T plots for the powder sample of **2**. This material is available free of charge via the Internet at http://pubs.acs.org.

IC048441X

(17) McConnell, H. M. *J. Chem. Phys.* **1963**, *39*, 1910.
(18) Unpublished results.
(19) (a) Feyerherm, R.; Mathoniere, C.; Kahn, O. *J. Phys.: Condens. Matter* **2001**, *13*, 2639. (b) Takagami, N.; Ishida, T.; Nogami, T. *Bull. Chem. Soc. Jpn.* **2004**, *77*, 1125.